



TITLE:

Enhancement of low-frequency spin-orbit-torque ferromagnetic resonance signals by frequency tuning observed in Pt/Py, Pt/Co, and Pt/Fe bilayers

AUTHOR(S):

Aoki, Motomi; Shigematsu, Ei; Matsushima, Masayuki; Ohshima, Ryo; Honda, Syuta; Shinjo, Teruya; Shiraishi, Masashi; Ando, Yuichiro

CITATION:

Aoki, Motomi ...[et al]. Enhancement of low-frequency spin-orbit-torque ferromagnetic resonance signals by frequency tuning observed in Pt/Py, Pt/Co, and Pt/Fe bilayers. *AIP Advances* 2021, 11(2): 025206.

ISSUE DATE:

2021-02

URL:

<http://hdl.handle.net/2433/276548>

RIGHT:

© 2021 Author(s).; All article content, except where otherwise noted, is licensed under a Creative Commons Attribution (CC BY) license.

Enhancement of low-frequency spin-orbit-torque ferromagnetic resonance signals by frequency tuning observed in Pt/Py, Pt/Co, and Pt/Fe bilayers

Cite as: AIP Advances **11**, 025206 (2021); <https://doi.org/10.1063/9.0000066>

Submitted: 14 October 2020 • Accepted: 23 December 2020 • Published Online: 02 February 2021

Motomi Aoki, Ei Shigematsu, Masayuki Matsushima, et al.

COLLECTIONS

Paper published as part of the special topic on [65th Annual Conference on Magnetism and Magnetic Materials](#)



View Online



Export Citation



CrossMark

ARTICLES YOU MAY BE INTERESTED IN

[Spin transfer torque devices utilizing the giant spin Hall effect of tungsten](#)

Applied Physics Letters **101**, 122404 (2012); <https://doi.org/10.1063/1.4753947>

[Spin-orbit torques: Materials, physics, and devices](#)

Applied Physics Letters **118**, 120502 (2021); <https://doi.org/10.1063/5.0039147>

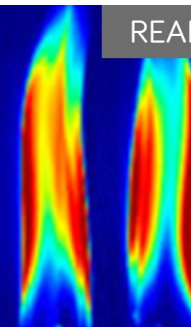
[Spin-orbit torque characterization in a nutshell](#)

APL Materials **9**, 030902 (2021); <https://doi.org/10.1063/5.0041123>

AIP Advances

Fluids and Plasmas Collection

READ NOW



AIP
Publishing

Enhancement of low-frequency spin-orbit-torque ferromagnetic resonance signals by frequency tuning observed in Pt/Py, Pt/Co, and Pt/Fe bilayers

Cite as: AIP Advances 11, 025206 (2021); doi: 10.1063/9.0000066
 Presented: 5 November 2020 • Submitted: 14 October 2020 •
 Accepted: 23 December 2020 • Published Online: 2 February 2021




View Online



Export Citation



CrossMark

Motomi Aoki,¹ Ei Shigematsu,¹ Masayuki Matsushima,¹ Ryo Ohshima,¹  Syuta Honda,²  Teruya Shinjo,¹
 Masashi Shiraishi,¹ and Yuichiro Ando^{1,a)}

AFFILIATIONS

¹Department of Electronic Science and Engineering, Kyoto University, Kyoto, Kyoto 615-8510, Japan

²Department of Pure and Applied Physics, Kansai University, Suita, Osaka 564-8680, Japan

Note: This paper was presented at the 65th Annual Conference on Magnetism and Magnetic Materials.

a) Author to whom correspondence should be addressed: ando@kuee.kyoto-u.ac.jp. Tel.: +81-75-383-2356. Fax: +81-75-383-2275. AI-226, Kyodai Katsura, Nishikyo-ku, Kyoto, Kyoto, Japan.

ABSTRACT

DC voltages via spin rectification effect (SRE), V_{DC} , under microwave irradiation are investigated for three platinum (Pt)/ferromagnetic metal (FM) bilayer structures: Pt/Ni₈₀Fe₂₀, Pt/Co, and Pt/Fe. At the microwave frequency region lower than the resonant frequency, large V_{DC} is obtained at zero DC magnetic field for all devices. In frequency dependence just around the resonant frequency, sharp rise and drop of magnitude in V_{DC} are observed. These behaviors are well explained by the numerically calculated magnetic susceptibility. It is also found that the magnitude of V_{DC} is strongly dependent on the slope of magnetoresistance spectrum. These findings lead to developments of sensitive detection technique for nano-scale magnetization switching.

© 2021 Author(s). All article content, except where otherwise noted, is licensed under a Creative Commons Attribution (CC BY) license (<http://creativecommons.org/licenses/by/4.0/>). <https://doi.org/10.1063/9.0000066>

Magnetization switching using spin-orbit torque (SOT)^{1–10} have been investigated intensively aiming at industrial production of SOT magneto-resistive random access memory (SOT-MRAM), because it has potential to realize both high durability and low power consumption at the same time. To this end, many researchers enthusiastically investigate materials with large spin Hall angle (SHA) such as heavy metals,^{1–3,5} topological insulators,^{4,6–8} Weyl semimetals,⁹ and oxide materials.¹⁰ There are several methods for quantification of SHA such as spin torque ferromagnetic resonance (ST-FMR),^{8,9,11} second harmonic method,^{4,10} spin absorption method,¹² and so on.^{13–15} Considering that our industrial goal is realization of efficient SOT switching, direct detection of magnetization switching should be straightforward and reliable. In this way, however, nano-fabrication of spin valve structure such as a magnetic tunnel junction is generally required, especially in case of a ferromagnet (FM) with in-plane magnetic anisotropy.^{2,3} Such additional and complicated

fabrication procedure impedes agile investigation of various materials. Kerr effect microscope can be also applicable to single FM layer without device fabrication, but it cannot be used to sub- μ m-scale FM because of its limited resolution.^{8,9}

Recently, highly sensitive detection of current induced magnetization switching of 100-nm-in-width FM with in-plane magnetic anisotropy was demonstrated by using low frequency ST-FMR (LFST-FMR).¹⁶ This method does not require any complicated fabrication procedures, allowing for agile research on SOT magnetization switching. In Ref. 16, however, the employed ferromagnet was limited to Ni₈₀Fe₂₀ (Py), and a comprehensive study on LFST-FMR using a wide variety of ferromagnets has yet to be investigated. Thus, the origin of LFST-FMR was not completely explained. In this study, we thoroughly investigate LFST-FMR by using three types of FM/NM devices, platinum (Pt)/Py, Pt/cobalt (Co), and Pt/iron (Fe). It is revealed that the slope of the magnetoresistance signals, i.e.,

resistance as a function of an external magnetic field, around zero magnetic field has a significant role in the magnitude of LFST-FMR. Furthermore, the LFST-FMR signals is enhanced under microwave with a specific frequency, indicating detection sensitivity of magnetization switching by LFST-FMR can be improved by choosing appropriate microwave frequency.

Figure 1(a) shows schematics of the device structure and electric circuit used in this study. First, a rectangular pattern was drawn by using electron beam (EB) lithography with a positive resist. Subsequently, MgO (2 nm)/FM (4 nm)/Pt (15 nm)/Ti (2 nm) layers were deposited by using EB deposition. The sample was exposed to the air and SiO₂ (6.7 nm) layer was deposited on the MgO layer by using RF magnetron sputtering to avoid the deliquescent of the MgO layer. After removing the resist, a

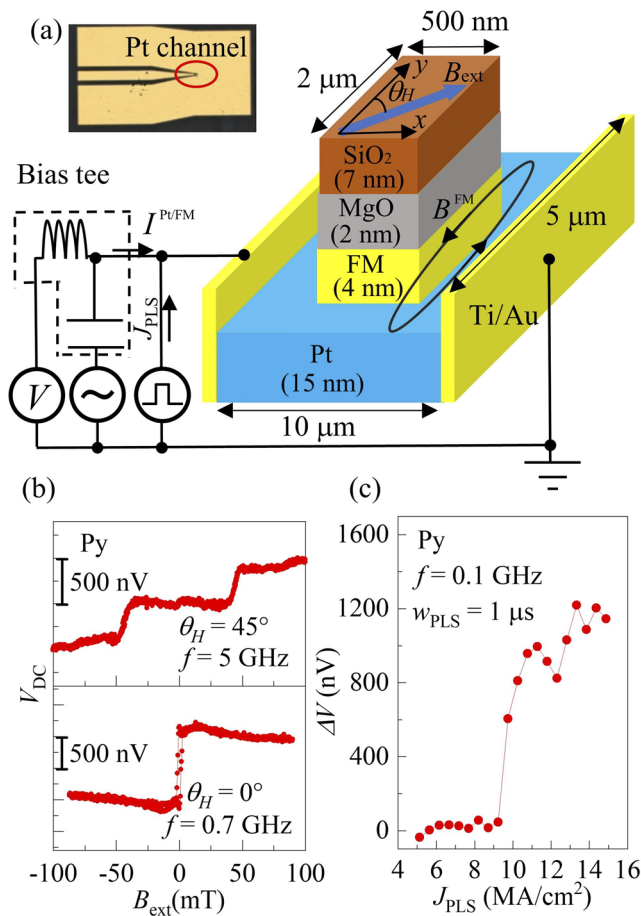


FIG. 1. (a) Schematics of the Pt channel and the measurement circuit for detecting spin torque ferromagnetic resonance (ST-FMR), low frequency ST-FMR (LFST-FMR), and magnetization switching spectra. Inset shows the picture of the whole device. Pt channel was fabricated in the region indicated by the red circle. (b) Upper panel shows ST-FMR spectrum at $\theta_H = 45^\circ$ and $f = 5$ GHz for the Pt/Py device. Lower panel shows LFST-FMR spectrum at $\theta_H = 0^\circ$ and $f = 0.7$ GHz for the Pt/Py. (c) ΔV as a function of J_{PLS} for the Pt/Py device at $f = 0.1$ GHz and $w_{PLS} = 1 \mu s$.

small rectangular pattern of FM electrode was drawn by using EB lithography with a negative resist. Then, argon ion (Ar⁺) milling was carried out and stopped after milling of FM layer in order to retain the Pt channel. Finally, Ti (3 nm)/Au (100 nm) coplanar wave guide was fabricated by using EB lithography and EB deposition. The width of the signal line and the separation with the ground line were 40 μm and 17 μm , which are narrowed down to 5 μm and 2.4 μm around the Pt channel [see the inset of Fig. 1(a)]. A microwave with a frequency, f , was applied by using commercial signal generator (KEYSHIGHT EXG analog signal generator N5173B) to excite magnetization oscillation. DC voltage via spin rectification effect (SRE), V_{DC} , was measured by using a nanovoltmeter (Keithley Nanovoltmeter 2187A). Microwave power, P_{MW} , was fixed to 5 dBm unless otherwise indicated. In the demonstration of current induced magnetization switching, pulse current (width: w_{PLS}) was applied by using a function generator (Agilent 33622A Waveform generator). All measurements were carried out at room temperature.

First, we demonstrated the detection of ST-FMR, LFST-FMR, and current induced magnetization switching. Fig. 1(b) shows ST-FMR and LFST-FMR spectra in the Pt/Py device. An external magnetic field, B_{ext} , was applied along the film plane with the angles, $\theta_H = 45^\circ$ for ST-FMR and $\theta_H = 0^\circ$ for the LFST-FMR, respectively. The magnitude of LFST-FMR was comparable to that of ST-FMR, consistent with our previous research.¹⁶ It is noted that V_{DC} in LFST-FMR signal shows two different voltage levels at 0 mT, corresponding to the magnetization direction. Therefore, we can demonstrate the current induced magnetization switching by measuring V_{DC} at 0 mT before and after the application of pulse current. Current induced magnetization switching signal obtained by using LFST-FMR is shown in Fig. 1(c). Difference in V_{DC} between before and after the application of pulse current at 0 mT, ΔV , was plotted as a function of the pulse current density, J_{PLS} . When J_{PLS} was larger than the threshold current density (9.5 MA/cm²), non-zero ΔV was observed, which indicates magnetization switching was successfully detected in this scheme. Because magnitude of signals in current induced magnetization switching is the same with that of hysteresis signals in the LFST-FMR measurements, hereafter we focus on the LFST-FMR signals.

Figures 2(a)-2(c) show LFST-FMR spectra of Pt/Py, Pt/Co, and Pt/Fe, respectively, at various frequencies. For all the devices, the magnitude of the signals was greatly enhanced under low frequency microwave irradiation, which is the typical characteristics of LFST-FMR. In case of Py/Pt, large LFST-FMR signal was obtained when f was lower than 2 GHz, consistent with our previous research.¹⁶ Meanwhile, large LFST-FMR signal appeared up to 7 GHz and 5 GHz in Pt/Co and Pt/Fe, respectively. The cause for the difference in the frequency dependence is attributed to ferromagnetic resonance (FMR) frequency, f_0 . According to the Kittel formula,¹⁷ f_0 is expressed as,

$$f_0 = \frac{\gamma}{2\pi} \sqrt{(B_{ext} + (N_x - N_y)\mu_0 M_s)(B_{ext} + (N_z - N_y)\mu_0 M_s)} \quad (1)$$

where γ , μ_0 , and M_s are gyrometric ratio, vacuum permeability, and saturation magnetization, respectively. N_x , N_y , N_z are demagnetization factor along x , y , and z direction, which are determined by the shape of FM electrode regardless of the species of FM, assuming the amorphous phase. According to Eq. (1), when $B_{ext} = 0$ mT, f_0 is

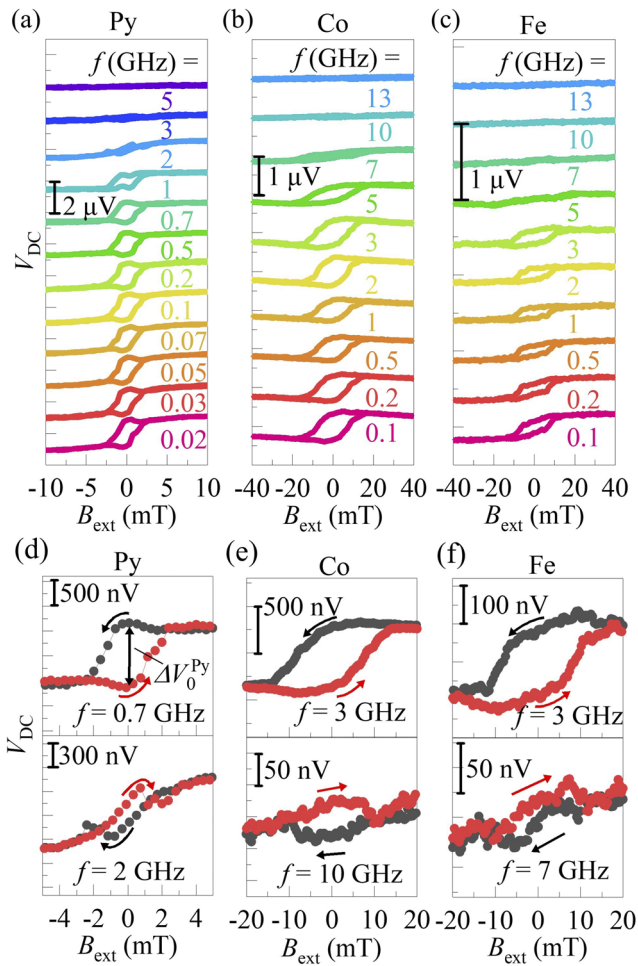


FIG. 2. LFST-FMR spectra with different f for the (a) Pt/Py, (b) Pt/Co, and (c) Pt/Fe devices. (d-f) The enlarged LFST-FMR signals around $B_{\text{ext}} = 0$ mT. The upper (lower) panels show signals at the low (high) frequencies.

proportional to M_s . M_s of Co and Fe are larger than that of Py as shown in Table I.^{18,19} Therefore, f_0 of Co and Fe are larger than that of Py, resulting in large LFST-FMR signals of Co and Fe observed at higher f , which is well explained by the magnetic susceptibility as mentioned later. Figure 2(d) shows an enlarged LFST-FMR signal of the Pt/Py device. Here we define $\Delta V_0^{\text{FM}} = V_{\uparrow} - V_{\downarrow}$, where V_{\uparrow} and V_{\downarrow} are V_{DC} at $B_{\text{ext}} = 0$ mT of down-sweep and up-sweep, respectively.

TABLE I. Parameters used in the micromagnetic simulation, M_s , α , and A_{ex} . f_0 obtained from the simulation by using these parameters is also shown.

FM	M_s (MA/m)	α	A_{ex} (pJ/m)	f_0 (GHz)
Py	0.46 ²⁴	0.008 ²²	13 ²⁴	1.43
Co	1.15 ¹⁸	0.011 ²²	19 ²¹	2.8
Fe	1.36 ¹⁹	0.0019 ²²	19 ²⁰	3

When $f = 0.7$ GHz, sign of ΔV_0^{Py} was positive. This is the same for signals in case that $f < 1$ GHz. In contrast, sign of ΔV_0^{Py} was negative when $f = 2$ GHz. Such sign reversal was also observed in the Pt/Co and Pt/Fe samples as shown in Fig. 2(e) and 2(f). Figure 3 shows ΔV_0^{FM} plotted as a function of f for the Pt/Py, Pt/Co, and Pt/Fe device. In addition to the aforementioned sign reversal, a peak of magnitude of ΔV_0^{FM} at around 3 GHz was observed in the Pt/Co and Pt/Fe samples with $P_{\text{MW}} = 5$ dBm. Whereas such a peak was not observed in the Pt/Py sample with $P_{\text{MW}} = 5$ dBm, a positive peak can be seen with the lower power, $P_{\text{MW}} = 0$ dBm, by mitigating a possible saturation of magnetic dynamics (see the inset of Fig. 3). Since the sensitivity of the measurement of current induced magnetization switching using LFST-FMR depends on the magnitude of ΔV_0^{FM} , the observed enhancement leads to realization of highly sensitive detection techniques by choosing appropriate frequencies.

To elucidate the background of these phenomena, i.e., sign reversal and peak in the frequency dependence of ΔV_0^{FM} , we now consider the magnetic susceptibility under microwave field. ΔV_0^{FM} is expressed as,²³

$$\Delta V_0^{\text{FM}} = 2\chi \langle I^{\text{Pt/FM}} \sin(2\pi ft) B^{\text{FM}} \frac{dR^{\text{Pt/FM}}}{dB_{\text{ext}}} \sin(2\pi ft - \varphi) \rangle, \quad (2)$$

where $\langle \rangle$ denotes the time average and χ is the absolute value of magnetic susceptibility normalized by that of $f \rightarrow 0$ GHz limit.¹⁷ $I^{\text{Pt/FM}}$ and B^{FM} are RF current and RF magnetic field induced by microwave. $R^{\text{Pt/FM}}$ and φ are the two terminal resistance of the whole device and the difference in the phase between the oscillation of the microwave current and the oscillation of the resistance, respectively. For easy discussion, here we consider only the contribution from the Oersted field via microwave, neglecting contribution from SOT via the spin Hall effect in the Pt layer. Considering susceptibility of ferromagnets around resonance, $\chi \sim 1$ and

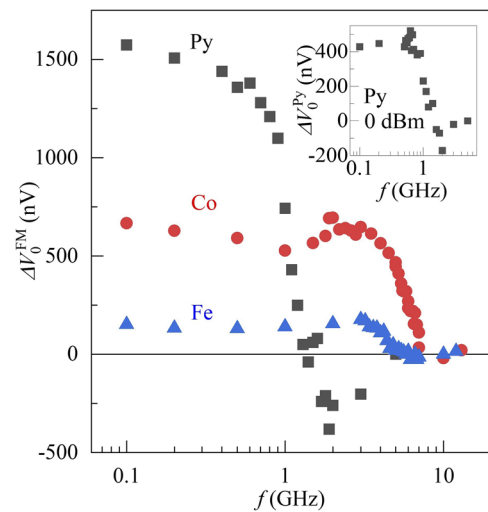


FIG. 3. ΔV_0^{FM} as a function of f at $P_{\text{MW}} = 5$ dBm for each sample. Inset shows the signal at $P_{\text{MW}} = 0$ dBm for the Pt/Py device.

$\varphi = 0^\circ$ at $f \ll f_0$, which yields positive ΔV_0^{FM} . χ increases as increasing f and reaches the maximum at $f = f_0$, which leads to an enhancement of the oscillation of the magnetization and the oscillation of the resistance as the result of magnetoresistance. One can simply expect ΔV_0^{FM} to increase monotonically as f approaches to f_0 from lower frequency. However, φ rapidly reaches 90° at the FMR condition, which suppresses the enhancement of ΔV_0^{FM} according to equation (2). Therefore, ΔV_0^{FM} reaches maximum at the frequency lower than f_0 . In the region where $f > f_0$, χ and φ approaches 0 and 180° , respectively. Thus, ΔV_0^{FM} decreases at the frequencies higher than f_0 and approaches zero when $f \gg f_0$. As for the sign inversion of ΔV_0^{FM} , however, no simple qualitative picture can be obtained from Eq. (2). To further investigate the magnetic susceptibility of each FM, we carried out micromagnetic simulation using *Mumax3*.²⁴ Parameters used in the micromagnetic simulation are shown in Table I, where α and A_{ex} are Gilbert damping constant and the exchange stiffness, respectively.^{18-22,24} Figures 4(a)-4(c) show χ and $\chi \cdot (\sin(2\pi ft) \sin(2\pi ft + \varphi))$ dependence on f . A clear peak in χ was found at $f = 1.43\text{GHz}$, 2.8GHz and 3GHz for Py, Co, and Fe, indicating FMR condition. The component, $\chi \cdot (\sin(2\pi ft) \sin(2\pi ft + \varphi))$, reaches the maximum when f is located at the point lower than f_0 , and it reverses its sign when f is higher than f_0 , indicating sign reversal in ΔV_0^{FM} . The simulated result well explains the frequency dependence of ΔV_0^{FM} including the sign inversion of ΔV_0^{FM} . However, the absolute value of the calculated positive peak in $\chi \cdot (\sin(2\pi ft) \sin(2\pi ft + \varphi))$ and that of the negative peak are almost the same, although the

experimentally observed positive and negative peaks of ΔV_0^{FM} were significantly different from each other as shown in Fig. 3. This difference is attributed to a possible contribution from anti-damping like torque, which is also detected as the symmetric component of a ST-FMR spectrum.¹¹ This contribution was neglected in our numerical calculations. In the Pt/FM devices, contribution from anti-damping like torque via the spin Hall effect in the Pt layer, which generates positive ΔV_0^{FM} around $f = f_0$, is substantial. In the measured devices, the SOT contribution can affect the magnetic dynamics, and consequently the ΔV_0^{FM} spectra may well be distorted.

Next, we focus on the relationship between magnetoresistance spectrum and the magnitude of LFST-FMR. Fig. 5 shows the two terminal resistance, $R^{\text{Pt/FM}}$, of each Pt/FM devices as a function of B_{ext} with $\theta_H = 0^\circ$. Insets show enlarged signals around $B_{\text{ext}} = 0$ mT and a schematic of measurement circuit. Because of the domain wall nucleation, $dR^{\text{Pt/FM}}/dB_{\text{ext}}$ has finite value around $B_{\text{ext}} = 0\text{mT}$ ^{23,25,26} even when B_{ext} is parallel to the easy axis of FM films. The observed values of $\Delta V_0^{\text{FM}}(f = 0.1\text{GHz})$, $I^{\text{Pt/FM}}$, B^{FM} and $dR^{\text{Pt/FM}}/dB_{\text{ext}}$ normalized by those of FM = Py case are shown in Table II along with the resistivity. Table II shows that $\Delta V_0^{\text{FM}}(f = 0.1\text{GHz})/\Delta V_0^{\text{Py}}(f = 0.1\text{GHz})$ becomes small as $\frac{dR^{\text{Pt/FM}}/dB_{\text{ext}}}{dR^{\text{Pt/Py}}/dB_{\text{ext}}}$ decreases monotonically by changing FM. As the other parameters related to the magnitude of $\Delta V_0^{\text{FM}}(f = 0.1\text{GHz})$, i.e., $I^{\text{Pt/FM}}$ and B^{FM} , were almost the same for all devices, $\Delta V_0^{\text{FM}}(f = 0.1\text{GHz})/\Delta V_0^{\text{Py}}(f = 0.1\text{GHz})$ seems to be dependent on $\frac{dR^{\text{Pt/FM}}/dB_{\text{ext}}}{dR^{\text{Pt/Py}}/dB_{\text{ext}}}$, which is consistent with Eq. (2). Note that if there is a finite slope in the resistance - B_{ext} curve, LFST-FMR can be obtained by LFST-FMR scheme. This indicates

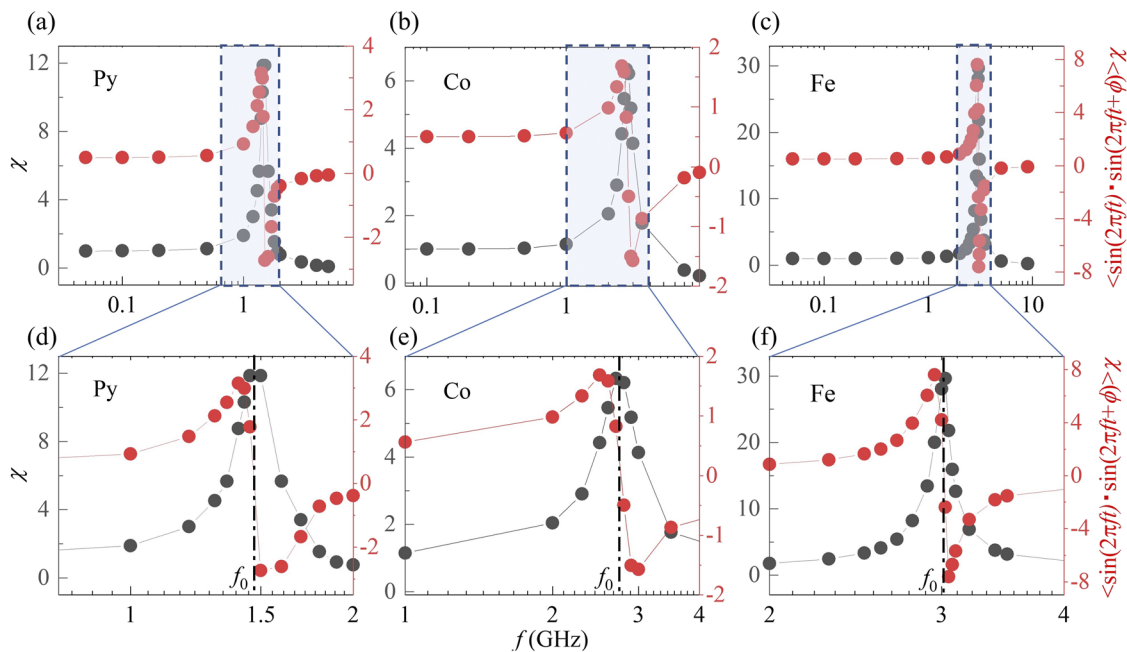


FIG. 4. χ and $\chi \cdot (\sin(2\pi ft) \sin(2\pi ft + \varphi))$ as a function of f obtained from the micromagnetic simulation for (a) Pt/Py, (b) Pt/Co, and (c) Pt/Fe device. Enlarged plots around $f = f_0$ for (d) Pt/Py, (e) Pt/Co, and (f) Pt/Fe device.

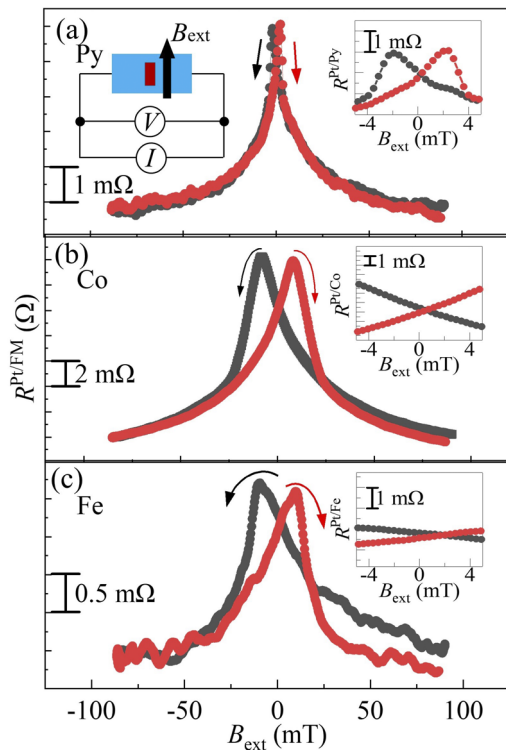


FIG. 5. R^{FM} as a function of B_{ext} for (a) Pt/Py, (b) Pt/Co and (c) Pt/Fe device. Enlarged signals around $B_{ext} = 0$ mT are shown in the inset. The measurement setup is also illustrated.

TABLE II. ΔV_0^{FM} , I^{FM} , B^{FM} , and $\frac{dR^{FM}}{dB_{ext}}$ at normalized by those of the Pt/Py device. I^{FM} and B^{FM} are estimated from the measured R^{FM} and ρ .

FM	$\Delta V_0^{FM} / \Delta V_0^{Py}$	ρ ($\mu\Omega$ cm)	$I^{Pt/FM} / I^{Pt/Py}$	B^{FM} / B^{Py}	$\frac{dR^{Pt/FM}}{dB_{ext}} / \frac{dR^{Pt/Py}}{dB_{ext}}$
Py	1	55	1	1	1
Co	0.41	72	1.01	1.03	0.75
Fe	0.09	58	0.99	0.99	0.13

that the detection method of current induced magnetization switching using LFST-FMR can be used for a wide variety of magnetic materials even including magnetic insulator bilayer such as YIG via spin Hall magnetoresistance²⁷ and 10-nm-scale FM/NM structure via magnon magnetoresistance.²⁸

In conclusion, LFST-FMR spectra of NM/FM structures with different FM materials were investigated. Magnitude of LFST-FMR was enhanced at a specific microwave frequency, the mechanism for which was well explained by the results of the micromagnetic simulations. Thus, it is indicated that the detection sensitivity of current induced magnetization switching can be much improved by choosing appropriate microwave frequency. We also found the slope of the resistance vs external magnetic field along easy axis of FM took a significant role in enhancement of LFST-FMR. Our findings suggest the sensitive detection method of current-induced magnetization

switching by using LFST-FMR is applicable to various kinds of materials including magnetic insulators and 10-nm-scale ferromagnetic metals.

This work was supported by JSPS (KAKENHI N. 16H06330, No. 19H02197, and No. 20H02607).

DATA AVAILABILITY

The data that support the findings of this study are available from the corresponding author upon reasonable request.

REFERENCES

- I. M. Miron, K. Garello, G. Gaudin, P.-J. Zermatten, M. V. Costache, S. Auffret, S. Bandiera, B. Rodmacq, A. Schuhl, and P. Gambardella, *Nature* **476**, 189 (2011).
- L. Liu, C.-F. Pai, Y. Li, H. W. Tseng, D. C. Ralph, and R. A. Buhrman, *Science* **336**, 555 (2012).
- C.-F. Pai, L. Liu, Y. Li, H. W. Tseng, D. C. Ralph, and R. A. Buhrman, *Applied Physics Letters* **101**, 122404 (2012).
- Y. Fan, P. Upadhyaya, X. Kou, M. Lang, S. Takei, Z. Wang, J. Tang, L. He, L.-T. Chang, M. Montazeri, G. Yu, W. Jiang, T. Nie, R. N. Schwartz, Y. Tserkovnyak, and K. L. Wang, *Nature Materials* **13**, 699 (2014).
- K. Garello, C. O. Avci, I. M. Miron, M. Baumgartner, A. Ghosh, S. Auffret, O. Boulle, G. Gaudin, and P. Gambardella, *Applied Physics Letters* **105**, 212402 (2014).
- M. De, R. Grassi, J. Y. Chen, M. Jamali, D. R. Hickey, D. Zhang, Z. Zhao, H. Li, P. Quarterman, Y. Lv, M. Li, A. Manchon, K. A. Mkhoyan, T. Low, and J. P. Wang, *Nature Materials* **17**, 800 (2017).
- K. Yasuda, A. Tsukazaki, R. Yoshimi, K. Kondou, K. S. Takahashi, Y. Otani, M. Kawasaki, and Y. Tokura, *Physical Review Letters* **119**, 137204 (2017).
- Y. Wang, D. Zhu, Y. Wu, Y. Yang, J. Yu, R. Ramaswamy, R. Mishra, S. Shi, M. Elyasi, K.-L. Teo, Y. Wu, and H. Yang, *Nature Communications* **8**, 1364 (2017).
- S. Shi, S. Liang, Z. Zhu, K. Cai, S. D. Pollard, Y. Wang, J. Wang, Q. Wang, P. He, J. Yu, G. Eda, G. Liang, and H. Yang, *Nature Nanotechnology* **14**, 945 (2019).
- L. Liu, Q. Qin, W. Lin, C. Li, Q. Xie, S. He, X. Shu, C. Zhou, Z. Lim, J. Yu, W. Lu, M. Li, X. Yan, S. J. Pennycook, and J. Chen, *Nature Nanotechnology* **14**, 939 (2019).
- L. Liu, T. Moriyama, D. C. Ralph, and R. A. Buhrman, *Physical Review Letters* **106**, 033601 (2011).
- M. Morota, Y. Niimi, K. Ohnishi, D. H. Wei, T. Tanaka, H. Kontani, T. Kimura, and Y. Otani, *Physical Review B* **83**, 174405 (2011).
- S. O. Valenzuela and M. Tinkham, *Nature* **442**, 176 (2006).
- K. Ando, S. Takahashi, J. Ieda, Y. Kajiwara, H. Nakayama, T. Yoshino, K. Harii, Y. Fujikawa, M. Matsuo, S. Maekawa, and E. Saitoh, *Journal of Applied Physics* **109**, 103913 (2011).
- C.-F. Pai, M. Mann, A. J. Tan, and G. S. D. Beach, *Physical Review B* **93**, 144409 (2016).
- M. Aoki, E. Shigematsu, M. Matsushima, R. Ohshima, S. Honda, T. Shinjo, M. Shiraishi, and Y. Ando, *Physical Review B* **102**, 174442 (2020).
- C. Kittel, *Physical Review* **73**, 155 (1947).
- S. P. Vermon, S. M. Lindsay, and M. B. Stearns, *Physical Review B* **29**, 4439 (1984).
- M. W. Grinstaff, M. B. Salamon, and K. S. Suslick, *Physical Review B* **48**, 269 (1993).
- S. M. Bhagat, L. L. Hirst, and J. R. Anderson, *Journal of Applied Physics* **37**, 194 (1966).
- C. Eyrich, W. Huttema, M. Arora, E. Montoya, F. Rashidi, C. Burrowes, B. Kardasz, E. Girt, B. Heinrich, O. N. Mryasov, M. From, and O. Karis, *Journal of Applied Physics* **111**, 07C919 (2012).

- ²²M. Oogane, T. Wakitani, S. Yakata, R. Yilgin, Y. Ando, A. Sakuma, and T. Miyazaki, *Japanese Journal of Applied Physics* **45**, 3889 (2006).
- ²³X. F. Zhu, M. Harder, J. Tayler, A. Wirthmann, B. Zhang, W. Lu, Y. S. Gui, and C. M. Hu, *Physical Review B* **83**, 140402(R) (2011).
- ²⁴A. Vansteenkiste, J. Leliaert, M. Dvornik, M. Helsen, F. G. Sanchez, and B. V. Waeyenberge, *AIP Advances* **4**, 107133 (2014).
- ²⁵V. D. Nguyen, P. Laczkowski, A. Marty, L. Notin, C. Beigné, L. Vila, and J. P. Attané, *Journal of Applied Physics* **115**, 053912 (2014).
- ²⁶D. Ruzmetov and V. Chandrasekhar, *Journal of Magnetism and Magnetic Materials* **320**, 47 (2008).
- ²⁷H. Nakayama, M. Althammer, Y.-T. Chen, K. Uchida, Y. Kajiyama, D. Kikuchi, T. Ohtani, S. Geprags, M. Opel, S. Takahashi, R. Gross, G. E. W. Bauer, S. T. B. Goennenwein, and E. Saitoh, *Physical Review Letters* **110**, 206601 (2013).
- ²⁸A. P. Mihai, J. P. Attane, A. Marty, P. Warin, and Y. Samson, *Physical Review B* **77**, 060401 (2008).